An ARID3A-dependent progenitor lineage confers developmental robustness to palate morphogenesis

Jie Gao[1,8], Litian Han[1,8], Yao Xiao[1,8], Yu Liang[1], Hongxu Tao[1], Qi Shi[1], Fei Pei[1], Zhaoming Wu[2], Yonghua Sun[3,4], Robert A. Cornell[5], Zhi Chen[1], Ophir D. Klein[5*], Huan Liu[1,6,7,9*]

[1] State Key Laboratory of Oral & Maxillofacial Reconstruction and Regeneration, Key Laboratory of Oral Biomedicine Ministry of Education, Hubei Key Laboratory of Stomatology, School & Hospital of Stomatology, Wuhan University, Wuhan 430079, China.

[2] Faculty of Dentistry, The University of Hong Kong, Hong Kong SAR, China

[3] State Key Laboratory of Freshwater Ecology and Biotechnology, Hubei Hongshan Laboratory, Institute of Hydrobiology, Innovation Academy for Seed Design, Chinese Academy of Sciences, Wuhan, China

[4] College of Advanced Agricultural Sciences, University of Chinese Academy of Sciences, Beijing, China

[5] Department of Oral Health Sciences, University of Washington, Seattle, WA USA

[6] Department of Pediatrics, Cedars-Sinai Guerin Children's, Los Angeles, CA 90048, USA.

[7] Frontier Science Center for Immunology and Metabolism, Wuhan University, China.

[8] TaiKang Center for Life and Medical Sciences, Wuhan University, China

[9] These authors contributed equally

[10] Lead contact

*Correspondence: Ophir D. Klein: Ophir.Klein@cshs.org;

Huan Liu: liu.huan@whu.edu.cn

Supplementary Figures

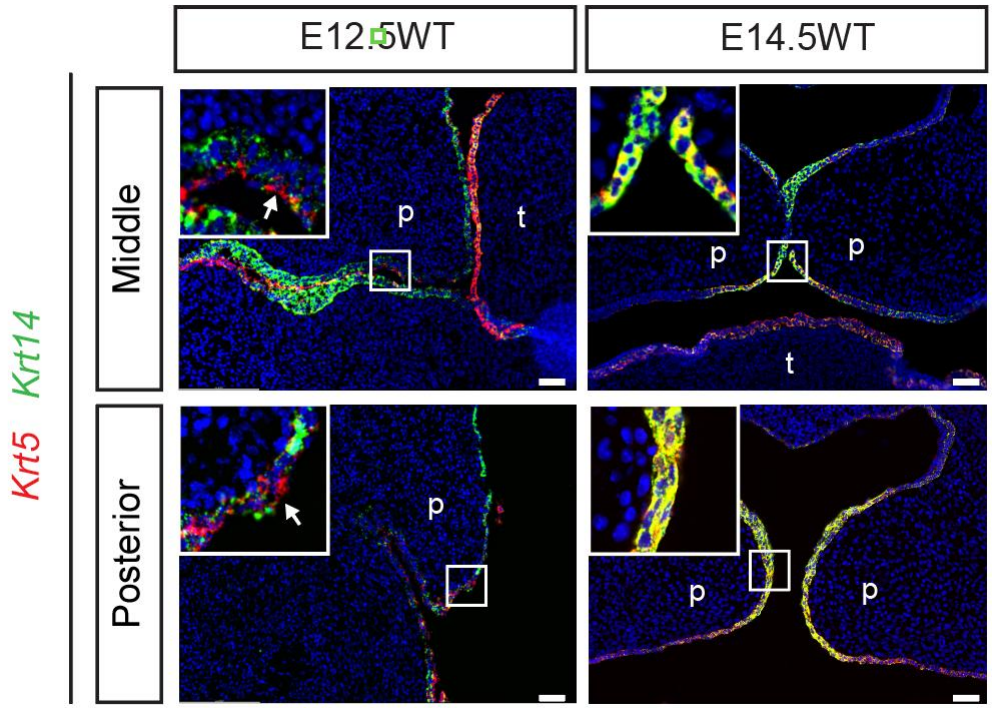

Figure S1. The expression pattern of *Krt5* and *Krt14* are different.

Dual RNAscope of *Krt5* with *Krt14* at E12.5 and E14.5 WT mouse palates. Each staining was performed at more than three different animals (N>3). ns, nasal septum; p, palatal shelf; t, tongue. Scale bar, 50μm.

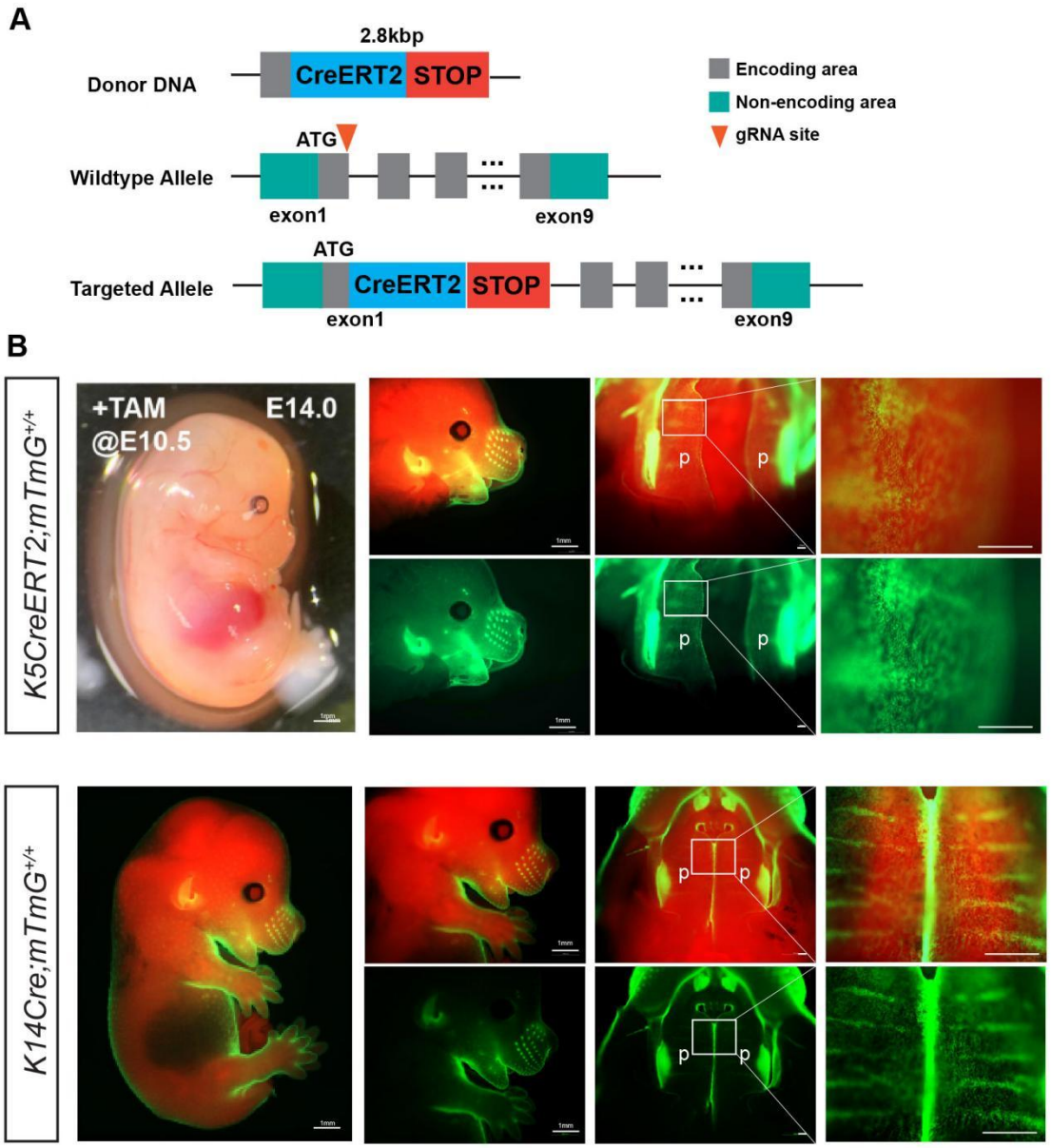

Figure S2. Both *K5CreERT2* and *K14*Cre mouse line could label periderm effectively.

(A) Schematic of the design and generation of *K5CreERT2;mTmG* mice.

(B) Representative fluorescence morphologies of E14.0 *K5CreERT2;mTmG* and *K14Cre;mTmG* mice. Tamoxifen(TM) was administered at E10.5. N≥3 mice in each timepoint were used. p, palatal shelf; t, tongue. Scale bar, 200μm.

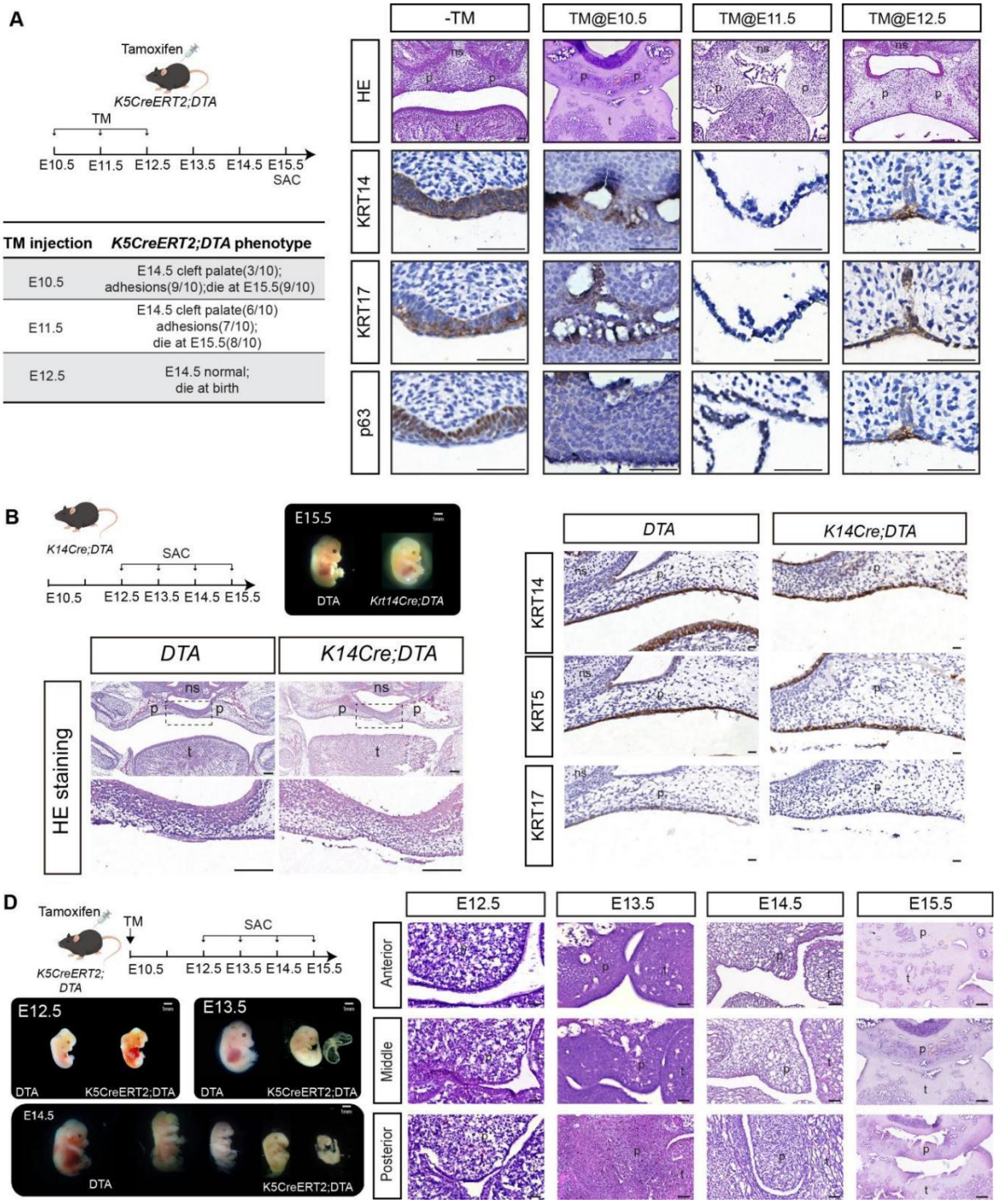

TM injection	*K5CreERT2;DTA* phenotype
E10.5	E14.5 cleft palate(3/10); adhesions(9/10);die at E15.5(9/10)
E11.5	E14.5 cleft palate(6/10) adhesions(7/10); die at E15.5(8/10)
E12.5	E14.5 normal; die at birth

Figure S3. Ablation of *K5*$^{+}$ and *K14*$^{+}$ lineages led to different phenotype.

(A) Schematic of the injection time of TM on *K5CreERT2;DTA* mice and tables of embryo phenotypes at *K5CreERT2;DTA* mice administered TM at E10.5 to E13.5. N≥3 mice in each timepoint were used. Representative H&E staining and immunohistochemistry analysis of KRT14, KRT17 and p63 at E15.5 *K5CreERT2;DTA* mice are shown on the right. ns, nasal septum; p, palatal shelf; t, tongue. Scale bar, 20μm.

(B) Schematic of the generation of *K14Cre;DTA* mice and morphologies of both *K14Cre;DTA* embryos exhibited limb malformation and DTA littermate embryos at E14.5.

N≥3 mice in each timepoint were used. ns, nasal septum; p, palatal shelf; t, tongue. Scale bar, 100μm.

(C) Representative H&E staining and immunohistochemistry analysis of KRT14, KRT17 and p63 at E15.5 *K14Cre;DTA* mice. Each staining was performed at more than three different animals (N>3). p, palatal shelf. Scale bar, 20μm.

(D) Schematic of generation and morphologies of *K5CreERT2;DTA* (E10.5TM) mice. N≥3 mice in each timepoint were used. Representative H&E staining of embryos harvested at different time are shown on the right. ns, nasal septum; p, palatal shelf; t, tongue. Scale bar, 20μm.

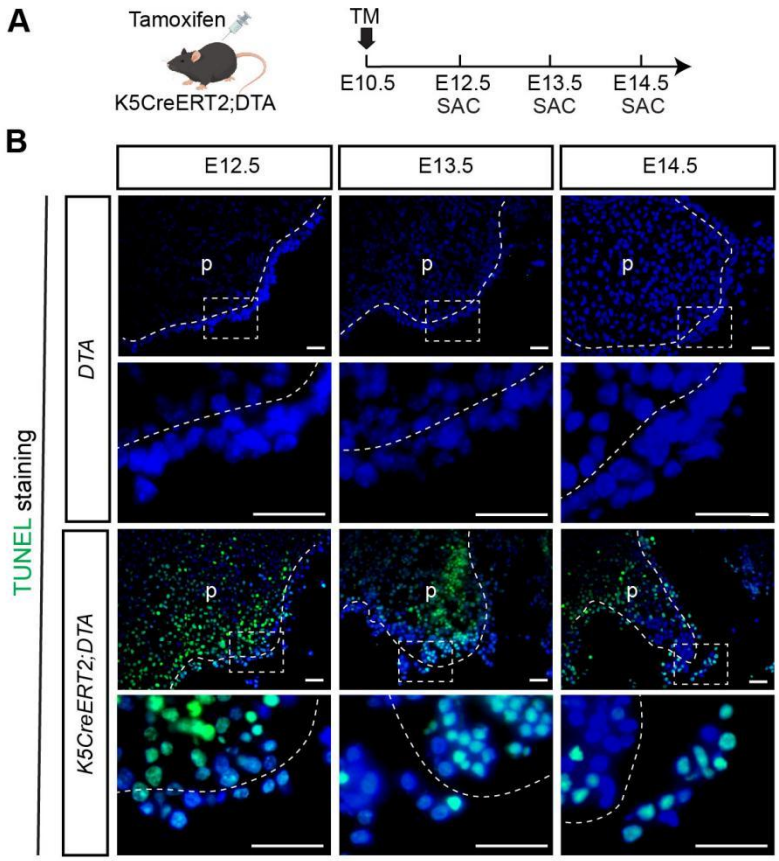

Figure S4. Ablation of *K5*$^{+}$ lineages led to death.

(A) Schematic of the generation of *K5CreERT2;DTA* mice (E10.5TM).

(B) TUNEL immunostaining of *DTA*, *K5CreERT2;DTA* (E10.5TM) mice at E12.5 - E14.5. Each staining was performed at more than three different animals (N>3). p, palatal shelf. Scale bar, 20μm.

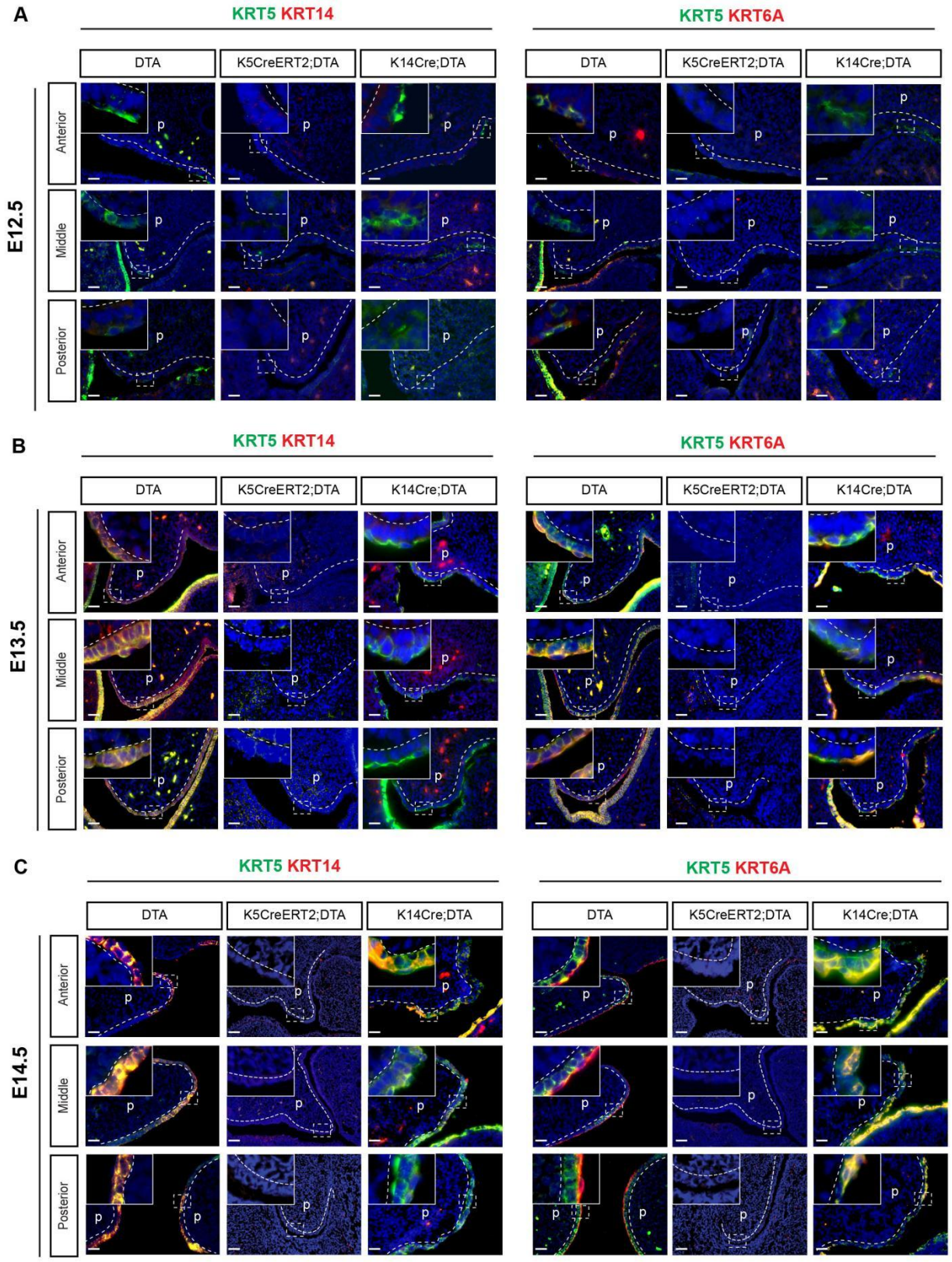

Figure S5. *K5*⁺ lineage cells showed differentiation capacity into the KRT14⁺ and KRT6A⁺ cells during E10.5-E12.5

(A-C) Dual immunostaining of KRT5 with KRT14 or KRT6A of *DTA*, *K5CreERT2;DTA*(E10.5TM) and *K14Cre;DTA* mice at E12.5(A), E13.5(B) and E14.5(C). Each staining was performed at more than three different animals (N>3). p, palatal shelf. Scale bar, 20μm.

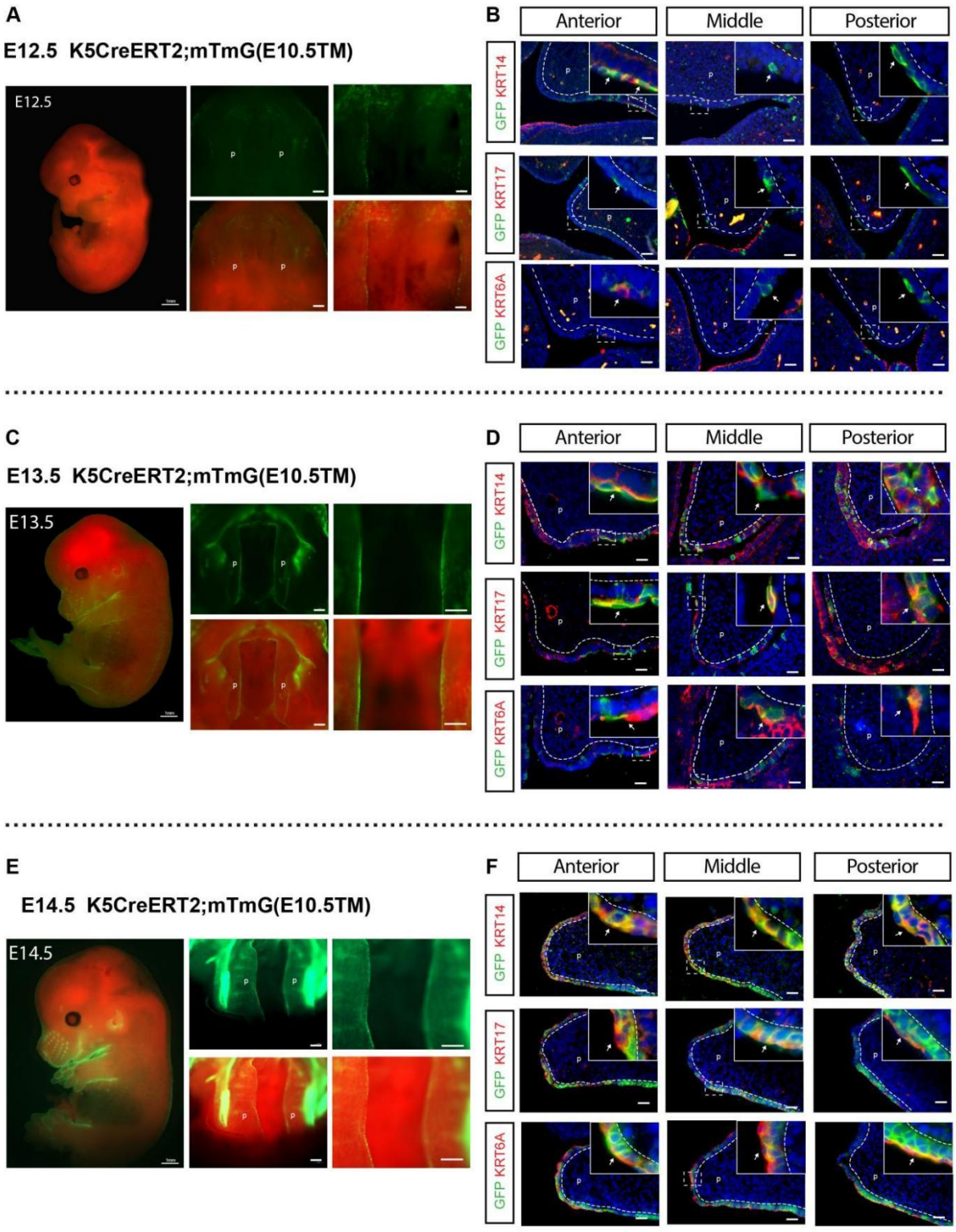

Figure S6. Temporal progression and differentiation of the *K5*$^{+}$ lineage in the developing embryo.

(A, C, E) Whole-mount fluorescence microscopy of *K5CreERT2;mTmG* embryos. Tamoxifen was administered at E10.5 to label *K5*$^{+}$ *lineage* cells, and embryos were harvested at E12.5 (A), E13.5(C), and E14.5 (E), showing the expansion of the GFP^{+} *K5* lineage over time. N≥3 mice in each timepoint were used. p, palatal shelf. Scale bar, 200μm.

(B, D, F) Corresponding immunofluorescence analysis on sections from the same embryos. Sections were co-stained to show the *K5*$^{+}$ lineage (GFP, green) and a keratin marker (KRT14, KRT17, KRT6A, red) at E12.5 (B), E13.5 (D), and E14.5 (F). Nuclei are counterstained with DAPI (blue). N≥3 mice in each timepoint were used. White arrows pointed to the periderm cells. p, palatal shelf. Scale bar, 20μm.

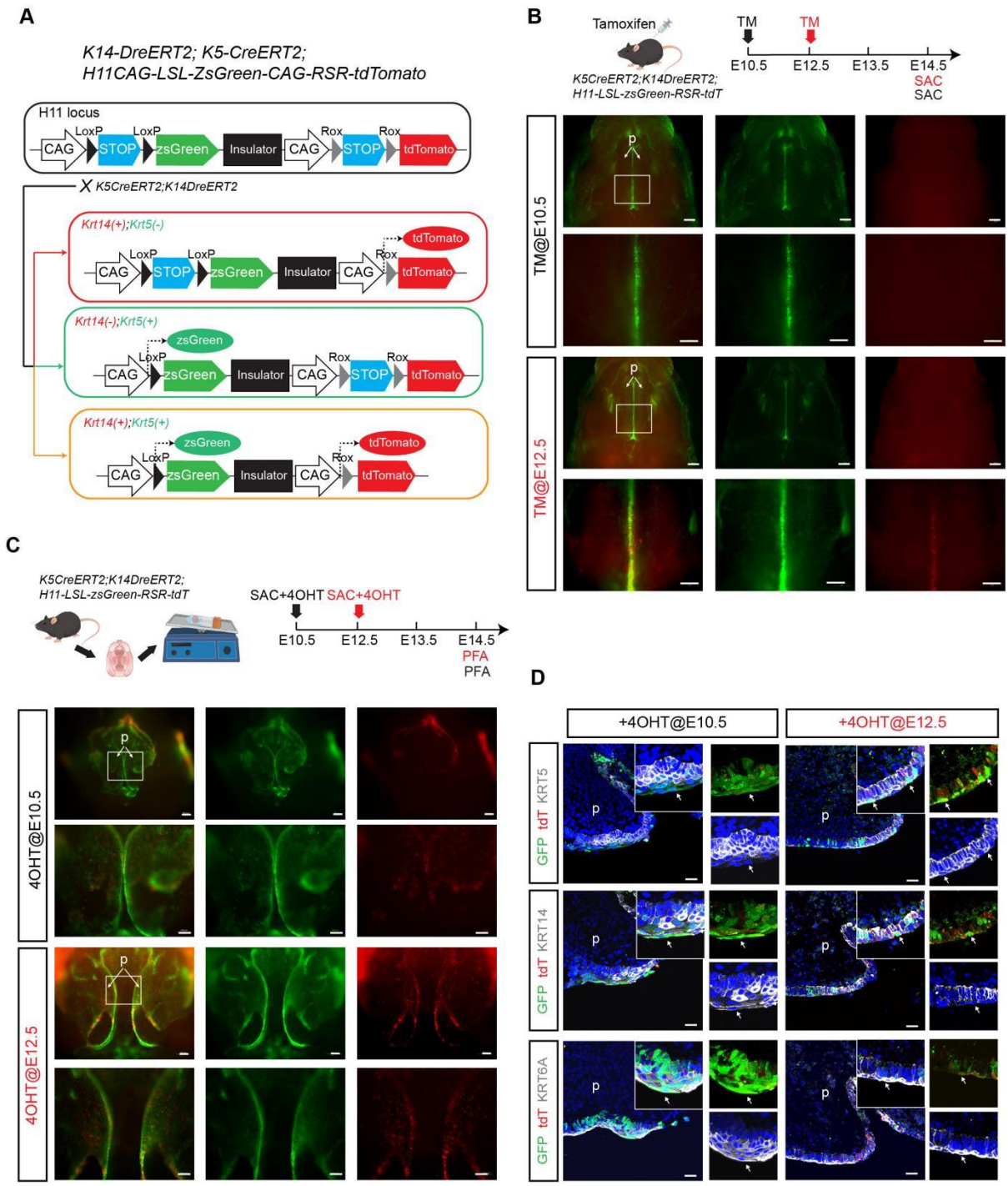

Figure S7. Dual-reporter mouse system distinguishes the fates of *K5*$^{+}$ and *K14*$^{+}$ lineage cells.

(A) Schematic of the dual-recombinase lineage tracing mouse model *K5CreERT2;K14DreERT2;H11*-CAG-LSL-H2B-EGFP-CAG-RSR-tdTomato(*K5;*

K14;H11). In this system, Cre activity (from the *Krt5* locus) alone permanently labels cells and their progeny with GFP. Dre activity (from the *Krt14* locus) alone permanently labels cells and their progeny with tdT.

(B) *In vivo* lineage tracing in the developing palate. TM was administered at E10.5 or E12.5, and embryos were harvested at E14.5. Representative whole-mount fluorescence images of dissected palatal shelves are shown at low (top) and high (bottom) magnification (n = 6 mice per condition). p, palatal shelf. Scale bar, 500μm.

(C) Ex vivo recapitulation of lineage dynamics using an explant culture system. Palatal shelves from E10.5 or E12.5 embryos were cultured with 4-hydroxytamoxifen (4-OHT) until a developmental stage equivalent to E14.5. Fluorescence morphology of cultured palates were showed at low (top) and high (bottom) magnification. N≥3 mice in each timepoint were used. p, palatal shelf. Scale bar, 500μm.

(D) Immunofluorescence analysis of cultured palatal explants. Sections were co-stained for the *K5*$^{+}$ lineage (GFP, green), the *K14*$^{+}$ lineage (tdT, red), and markers for keratin markers (KRT5, KRT14 and KRT6A) epithelial cells (gray). Nuclei were counterstained with DAPI (blue). Each staining was performed at more than three different animals (N>3). White arrows pointed to the periderm cells. p, palatal shelf. Scale bars, 20 μm.

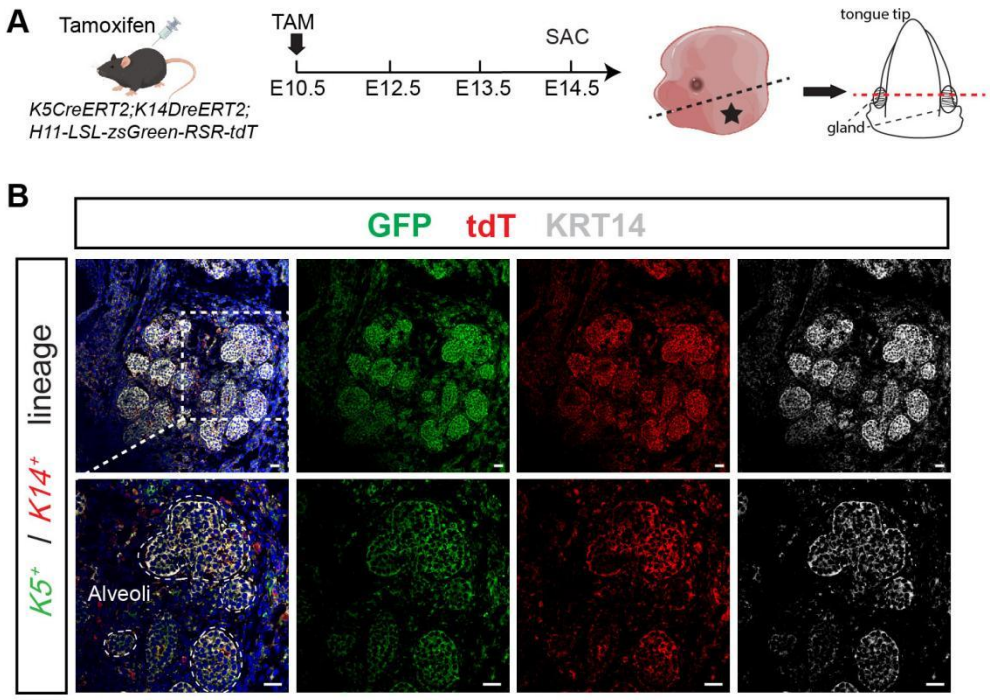

Figure S8. Both *K5*⁺ lineage and *K14*⁺ lineage cells could be normally labelled in the salivary glands.

Immunofluorescence analysis of *K5; K14;H11* mouse salivary glands. Sections were co-stained for the *K5*⁺ lineage (GFP, green), the *K14*⁺ lineage (tdT, red), and KRT14 (gray). Each staining was performed at more than three different animals (N>3). White dashes showed the structure of alveoli. Scale bars, 20 μm.

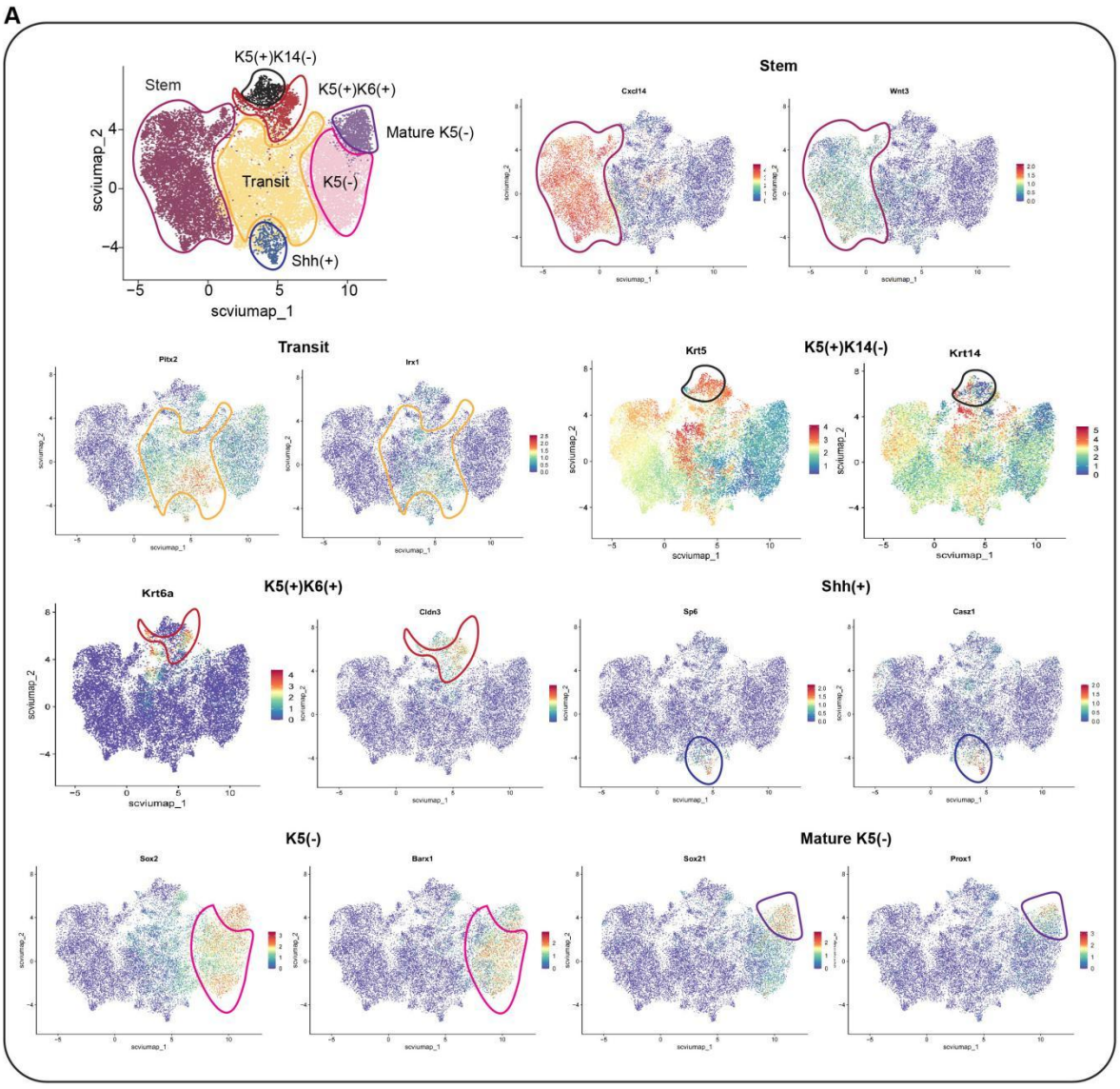
A
K5(+)K14(-)
Stem
K5(+)K6(+)
Mature K5(-)
Transit
K5(-)
Shh(+)
scviumap_2
scviumap_1
Stem
Cxcl14
Wnt3
Transit
Pitx2
Irx1
K5(+)K14(-)
Krt5
Krt14
K5(+)K6(+)
Krt6a
Cldn3
Shh(+)
Sp6
Casz1
K5(-)
Sox2
Barx1
Mature K5(-)
Sox21
Prox1

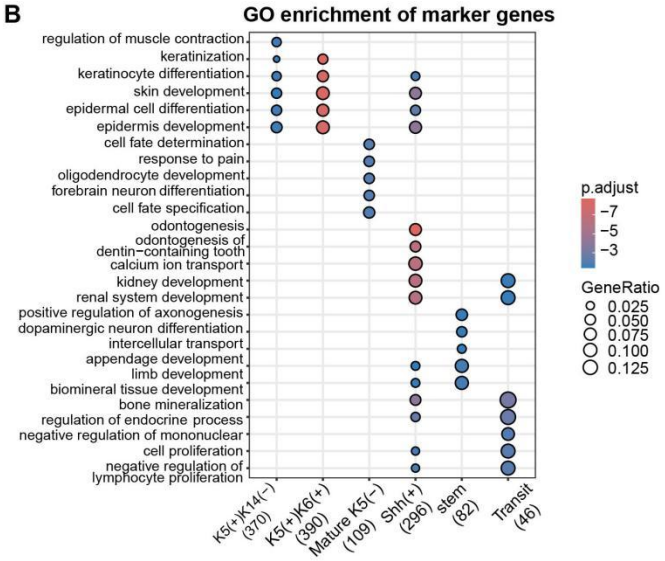
B
GO enrichment of marker genes
regulation of muscle contraction
keratinization
keratinocyte differentiation
skin development
epidermal cell differentiation
epidermis development
cell fate determination
response to pain
oligodendrocyte development
forebrain neuron differentiation
cell fate specification
odontogenesis
odontogenesis of dentin-containing tooth
calcium ion transport
kidney development
renal system development
positive regulation of axonogenesis
dopaminergic neuron differentiation
intercellular transport
appendage development
limb development
biomineral tissue development
bone mineralization
regulation of endocrine process
negative regulation of mononuclear
cell proliferation
negative regulation of lymphocyte proliferation
K5(+)K14(-) (370)
K5(+)K6(+) (390)
Mature K5(-) (109)
Shh(+) (296)
stem (82)
Transit (46)
p.adjust
−7
−5
−3
GeneRatio
0.025
0.050
0.075
0.100
0.125

Figure S9. Single-cell transcriptional profiling of different clusters.

(A) Feature plots displaying the expression of representative marker genes for each major cell cluster. Different circles indicate the positions of different clusters.

(B) Dot plot displaying enriched Gene Ontology (GO) terms for the marker genes defining each cell cluster.

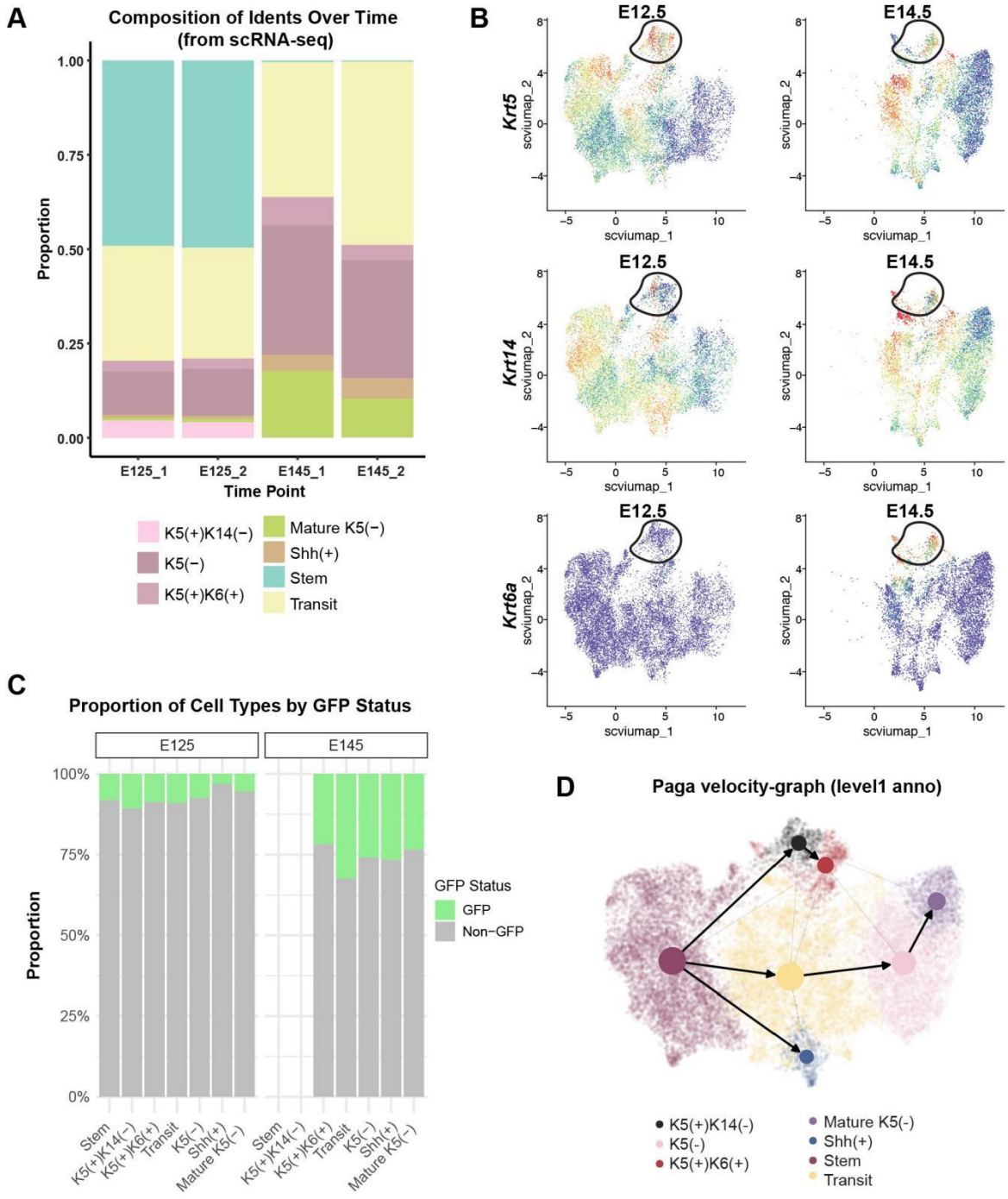

Figure S10. The cluster of K5^{+}K14^{-} cells was specifically presented in E12.5 .

(A) Bar plot comparing the cellular composition between the E12.5 and E14.5 developmental timepoints. Each bar represents a sample, with colored segments corresponding to the relative proportion of each identified cell type.

(B) Comparative visualization of gene expression in the E12.5 (left) and E14.5 (right) datasets. Feature plots display the expression patterns of *Krt6a*, *Krt5*, and *Krt14* on UMAP embeddings.

(C) Proportion of cell types by GFP status.

(D) RNA velocity analysis using scVelo, projecting cellular transitions and differentiation trajectories onto the Uniform Manifold Approximation and Projection (UMAP) embedding.

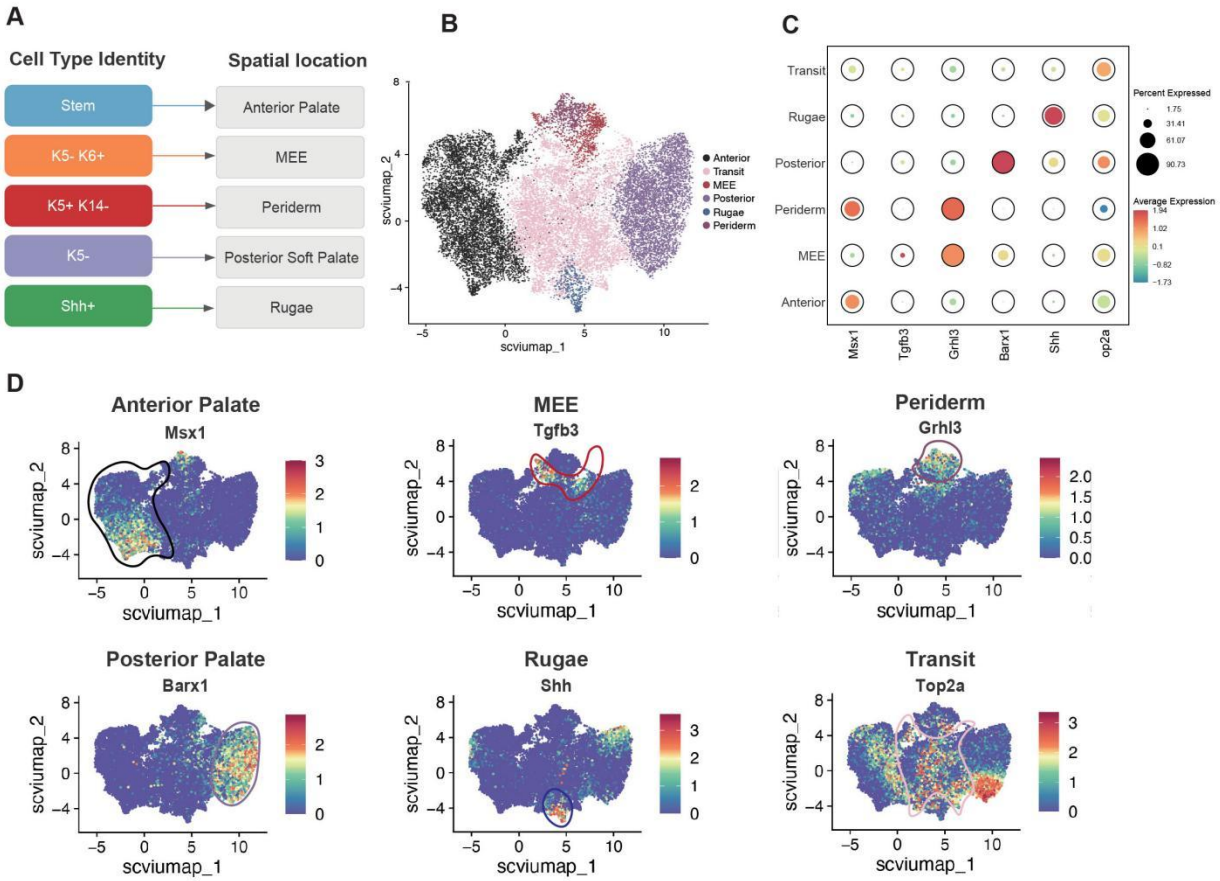

142

143 **Figure S11. The spatial localization patterns of cell type annotations.**

144 (A) The correspondence between our cell types and established cell types based on
145 regional markers.

146 (B) UMAP visualization of our re-annotated datas. Cells are colored by their assigned
147 clusters.

148 (C) Dot plot showing the average expression level (color intensity) and the percentage
149 of expressing cells (dot shape) of marker genes for each new cell cluster.

150 (D) Feature plots displaying the expression of representative marker genes for each cell
151 cluster. Different circles indicate the positions of different clusters.

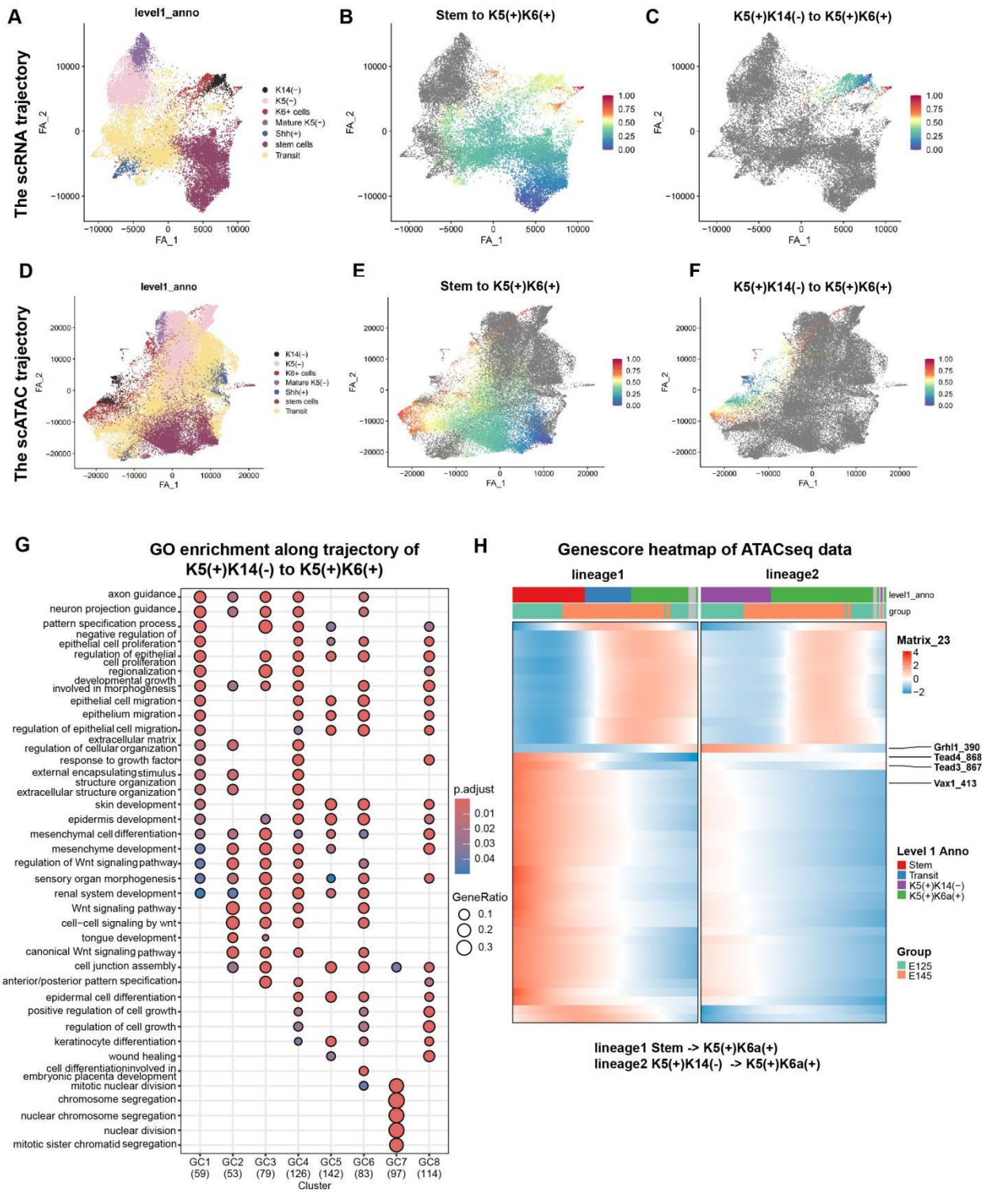

Figure S12. Single-cell transcriptional profiling of the trajectory of *K5(+)K14(-)* cells to *K5(+)K6(+)* cells

(A, D) Force-directed graph embeddings of the scRNA-seq (A) and scATAC-seq (D) datasets.

(B, E) Visualization of the **"Stem to K5^{+}K6^{+}"** differentiation trajectory within the scRNA-seq (B) and scATAC-seq (E) data. Cells belonging to this lineage are highlighted and colored by their inferred pseudotime, from early (blue) to late (yellow).

(C, F) Pseudotemporal ordering of the "**K5^{+}K14- to K5^{+}K6^{+}**" lineage within the scRNA-seq (C) and scATAC-seq (F) data, with cells colored by developmental progression.

(G) Dot plot displaying enriched Gene Ontology (GO) terms for the dynamic gene clusters identified along the differentiation trajectory (from Figure 3I). Dot size corresponds to the gene count, and color indicates statistical significance.

(H) Heatmap showing dynamic changes in transcription factor (TF) motif accessibility along the **K5^{+}K6^{+}** Periderm lineage, as inferred from the scATAC-seq data.

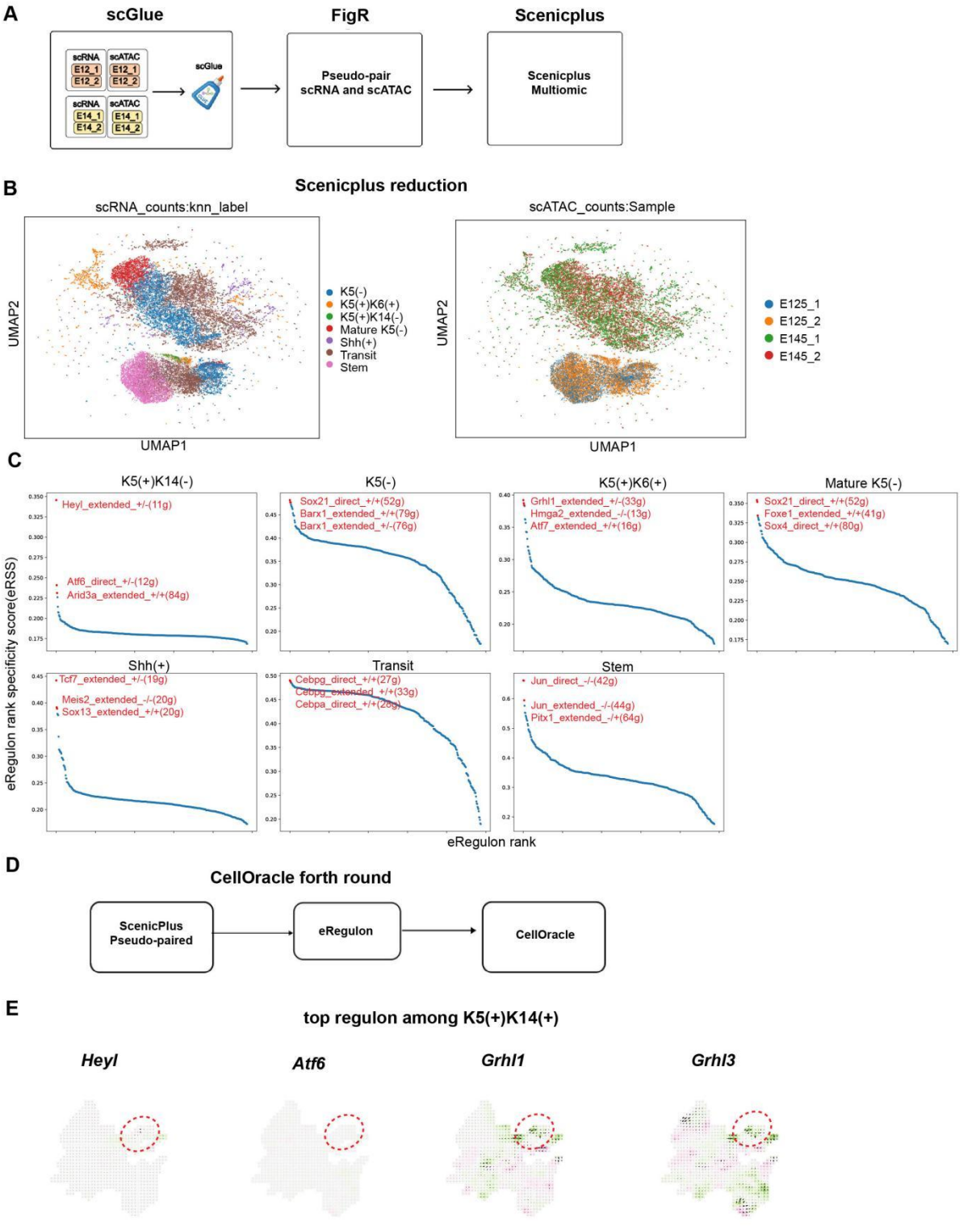

FigureS13. Integrative analysis based on scRNA-seq and scATAC-seq predicting top TFs related with different palatal epithelial cell differentiation.

(A) Scheme showing integration of scRNA-seq and scATAC-seq based on scGlue and FigR for pseudo-pairing of the two profiles.

(B) SCENIC+ based integration and reduction, cell populations were projected to UMAP plot

(C) Scatter plots for SCENIC+ based eRegulon rank specificity scores for different cell populations. Top three TFs are highlighted in the plots.

(D) CellOracle pipeline: The top regulons/TFs predicted by SCENIC^{+} were subjected to CellOracle prediction.

(E) Perturbation results of the top regulons (except *Arid3a*) within *K5*$^{+}$*K14*$^{-}$ population.

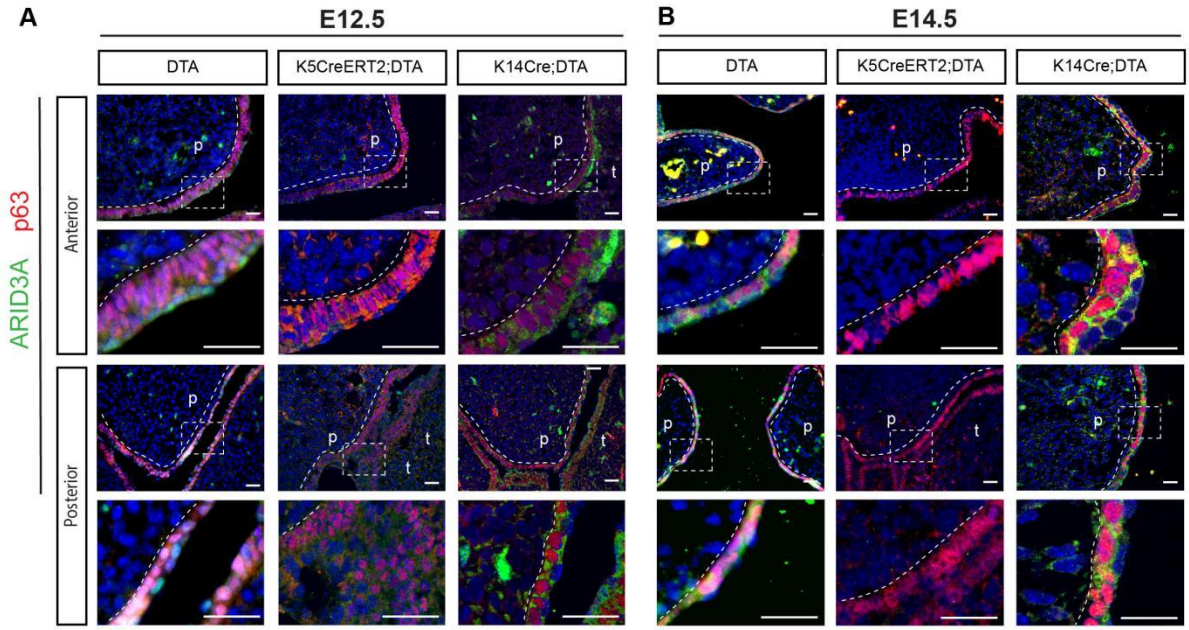

Figure S14. Expression pattern of ARID3A in palate epithelium.

Dual immunofluorescence analysis of ARID3A with p63 at E12.5(A) and E14.5(B) DTA, *K5CreERT2;DTA* and *K14Cre;DTA* mice palates including anterior and posterior palates. Sections were co-stained to show the expression of ARID3A(green) and p63(red). Nuclei are counterstained with DAPI (blue). Each staining was performed at more than three different animals (N>3). White arrows pointed to the periderm cells. p, palatal shelf; t, tongue. Scale bars, 20 μm.

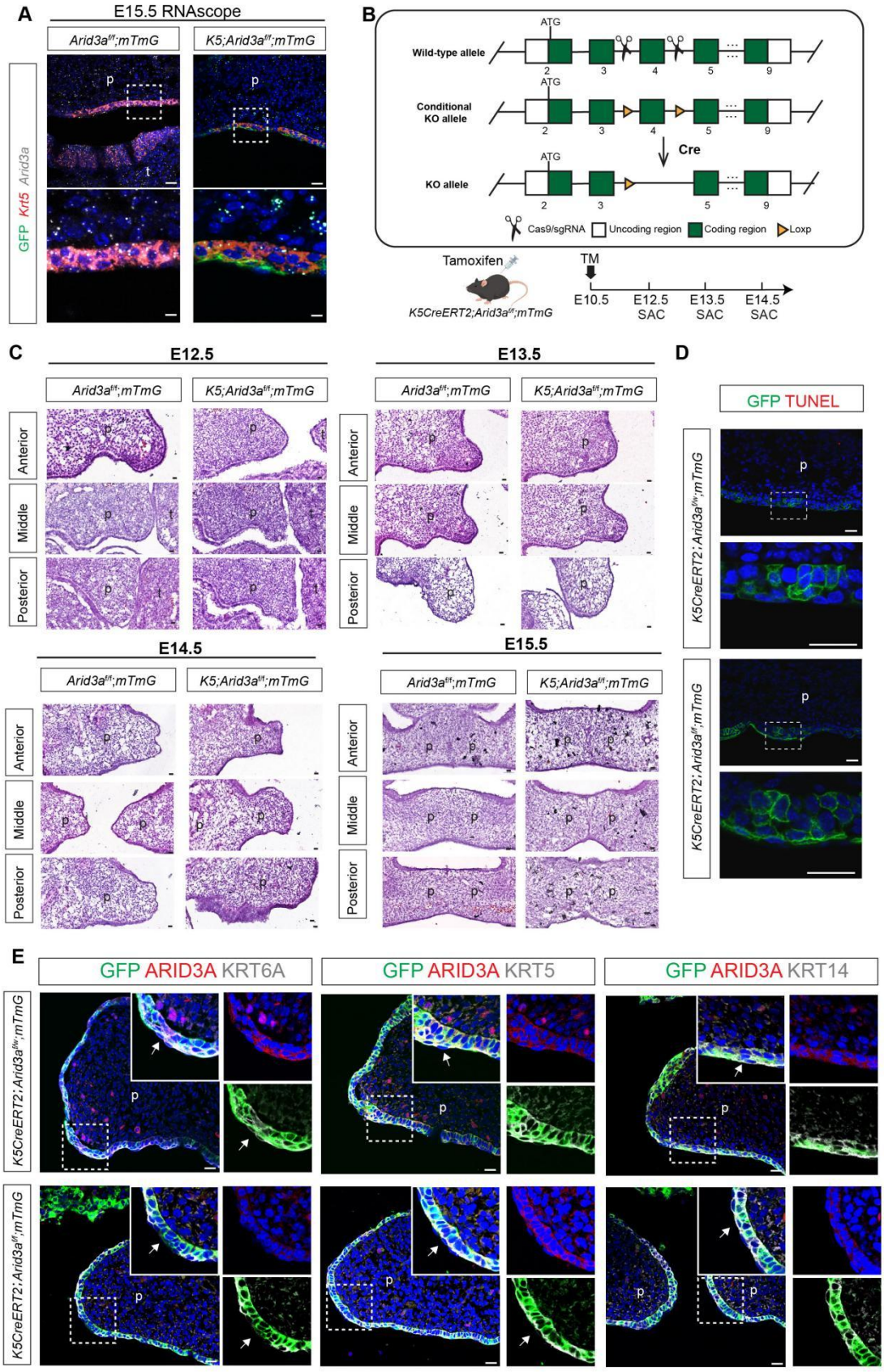
A
E15.5 RNAscope
Arid3a^f/f;mTmG
K5;Arid3a^f/f;mTmG
GFP Krt5 Arid3a
B
Wild-type allele
Conditional KO allele
KO allele
ATG
Cre
Cas9/sgRNA
Uncoding region
Coding region
Loxp
Tamoxifen
TM
K5CreERT2;Arid3a^f/f;mTmG
E10.5
E12.5 SAC
E13.5 SAC
E14.5 SAC
C
E12.5
E13.5
E14.5
E15.5
Anterior
Middle
Posterior
D
GFP TUNEL
K5CreERT2;Arid3a^f/+;mTmG
K5CreERT2;Arid3a^f/f;mTmG
E
GFP ARID3A KRT6A
GFP ARID3A KRT5
GFP ARID3A KRT14
K5CreERT2;Arid3a^f/+;mTmG
K5CreERT2;Arid3a^f/f;mTmG

Figure S15. Loss of ARID3a resulted in a delay in palatal development in vivo.

(A) RNAscope *in situ* hybridization for *Arid3a* (gray) and *Krt5* (red) transcripts in palatal shelves of *Arid3a$^{f/f}$;mTmG* and *K5CreERT2;Arid3a$^{f/f}$;mTmG* embryos at E15.5. The mTmG reporter confirms Cre-mediated recombination in *K5*$^{+}$ epithelial cells(green). Representative picture of N≥3 per group. p, palatal shelf; t, tongue. Scale bar, 20 μm.

(B) Schematic of the strategy for generating the *Arid3a* conditional knockout allele and the experimental timeline. LoxP sites were inserted flanking exon 4 of the *Arid3a* gene using a dual-sgRNA/Cas9 approach. Tamoxifen was administered to pregnant *K5CreERT2;Arid3a$^{f/f}$;mTmG* mices at E10.5. Embryos were harvested for analysis at E12.5 to E15.5.

(C) Representative H&E staining images of *Arid3a$^{f/f}$;mTmG* and *K5CreERT2;Arid3a$^{f/f}$;mTmG* mice palates at E12.5 to E15.5. N≥3 mice in each timepoint were used. p, palatal shelf; t, tongue. Scale bar, 20 μm.

(D) TUNEL staining of *K5CreERT2;Arid3a$^{f/w}$;mTmG and K5CreERT2;Arid3a$^{f/f}$;mTmG* embryos at E14.5. High-magnification images were shown below. Representative picture of N≥3 per group. p, palatal shelf. Scale bar, 20 μm.

(E) Immunofluorescence co-staining for GFP (recombined cells), ARID3A, and keratin markers (KRT5, KRT14, KRT6a) in E14.5 palatal shelves. Note the loss of ARID3A in the GFP^{+} epithelium of CKO mice and the discontinuous expression pattern of the differentiation marker *Krt6a* (white arrows). Representative picture of N≥3 per group. p, palatal shelf. Scale bar, 20 μm.

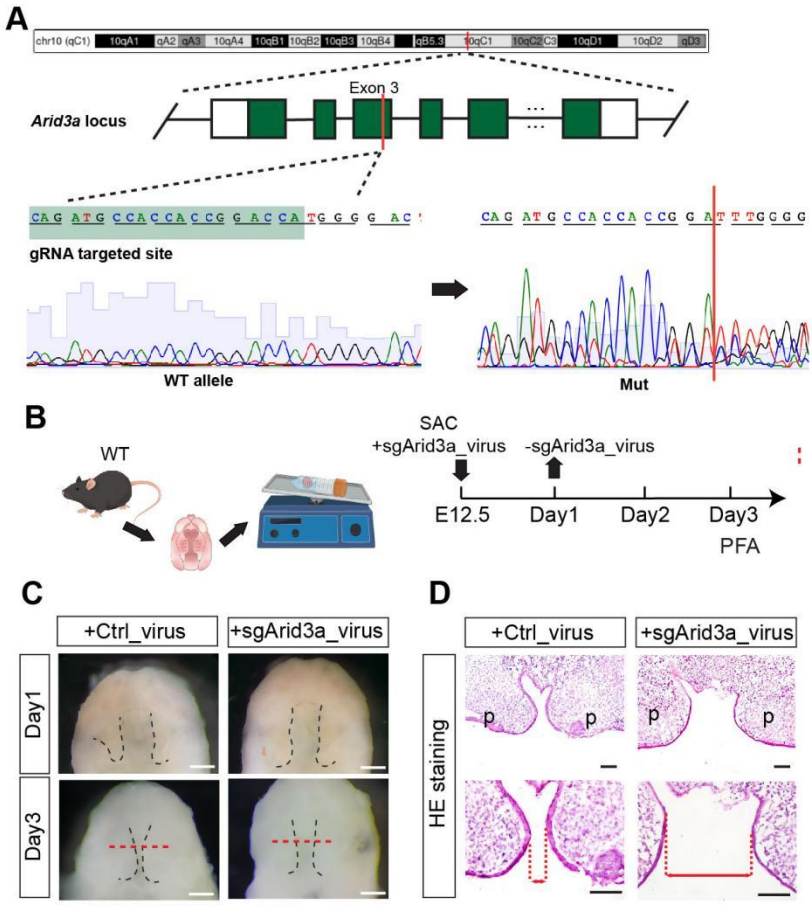

Figure S16. Loss of ARID3a resulted in a delay in palatal development ex vivo.

(A) Schematic of the *ex vivo* palate culture model. Palatal shelves were dissected from E12.5 wild-type embryos. The shelves were then transduced with lentiviruses expressing either a control sgRNA (Ctrl) or an sgRNA targeting *Arid3a* (sgArid3a). After 24 hours, the viral medium was replaced, and the shelves were cultured for 3 days before being fixed and harvested for analysis. N = 6 biological replicates per condition.

(B) Gross morphology of cultured palatal shelves on day 3. Shelves treated with sgArid3a lentivirus show impaired growth and fusion compared to Ctrl-treated shelves. Scale bar, 1mm.

(C) H&E staining of cultured palatal shelves on day 3. Top panels show low-magnification views, and bottom panels show high-magnification views. The red dashed line indicates the distance between the opposing palatal shelves, highlighting the fusion failure in the sgArid3a group. Representative picture of N≥3 per group. p, palatal shelf. Scale bar, 100 μm.

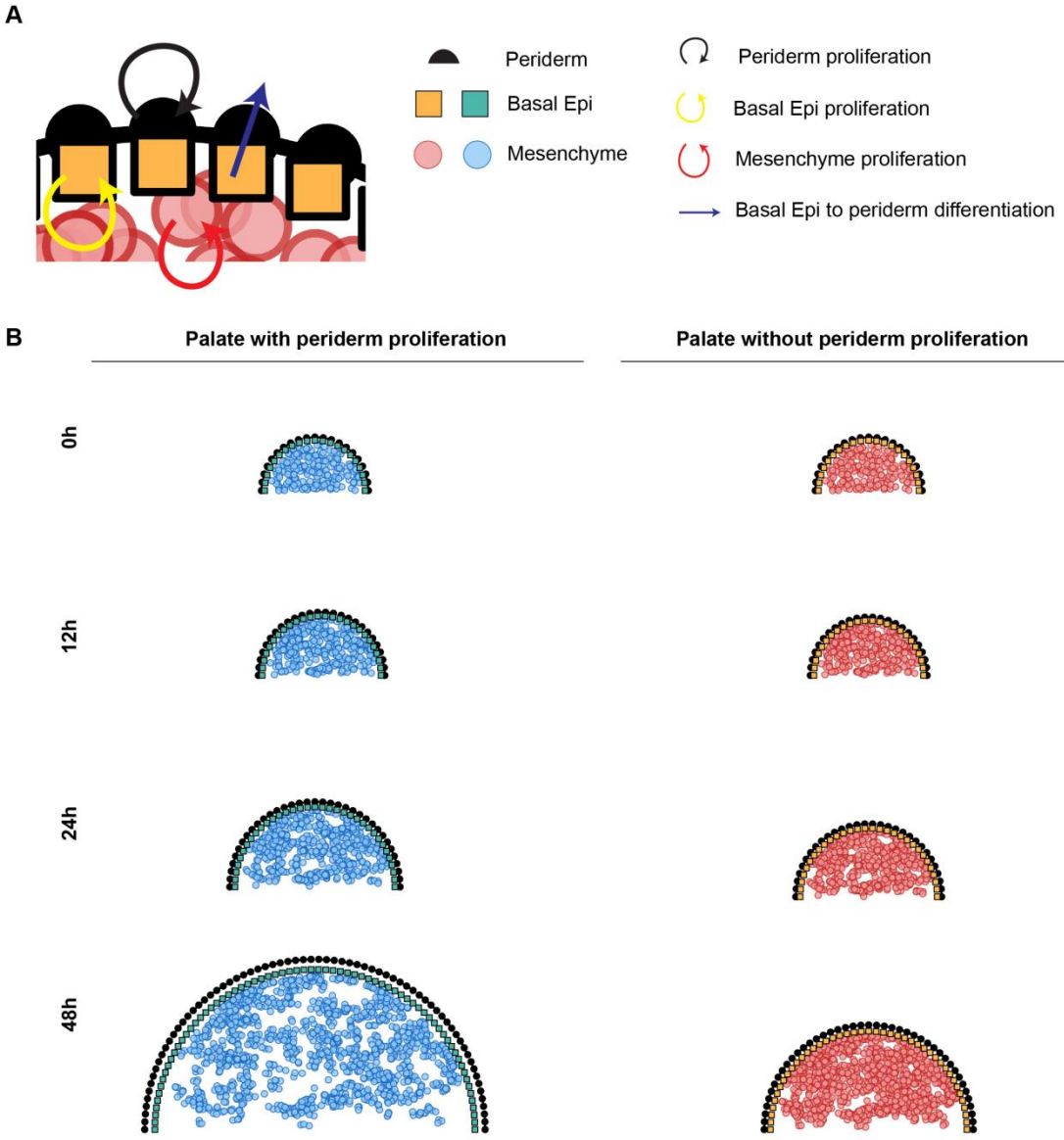
A
Periderm
Basal Epi
Mesenchyme
Periderm proliferation
Basal Epi proliferation
Mesenchyme proliferation
Basal Epi to periderm differentiation
B
Palate with periderm proliferation
Palate without periderm proliferation
0h
12h
24h
48h
C
Avg Nearest Neighbor Distance Over Time
with proliferation
without proliferation
Distance (um)
Time (hours)

Figure S17. Mathematical modeling demonstrates that periderm proliferation is essential for coordinating palatal growth.

(A) Schematic of the agent-based stochastic model interactions. The model incorporates three cell populations: periderm (black), basal epithelium (yellow squares), and mesenchyme (circles). Key dynamic processes include: (1) Self-renewal of all three cell types (curved arrows), and (2) Differentiation of basal epithelial cells into periderm cells (blue arrow). This framework allows for the simulation of tissue growth driven by the balance between internal mesenchymal proliferation and external boundary expansion.

(B) Time-lapse simulation of palate outgrowth over 48 hours. (Left) In the "Palate with periderm proliferation" model (Control condition), active periderm self-renewal allows the epithelial boundary to expand coordinately with the proliferating mesenchyme (blue), resulting in substantial radial growth and maintenance of normal cell density. (Right) In the "Palate without periderm proliferation" model (consistent with the Arid3a cKO condition), the loss of periderm self-renewal restricts boundary expansion. Despite normal mesenchymal proliferation (red), the physical constraint leads to stunted outgrowth and progressive mesenchymal crowding from 0h to 48h.

(C) Temporal evolution of spatial crowding. Time-course quantification of the Average Nearest Neighbor Distance (NND) between mesenchymal cells over 48 hours. In the "Palate with periderm proliferation" model (blue line), the NND progressively increases, reflecting sufficient spatial expansion and reduced cell density. Conversely, in the "Palate without periderm proliferation" model (red line), the NND steadily decreases, quantitatively confirming progressive cellular crowding due to restricted boundary expansion. Solid lines represent the mean, and shaded regions indicate the standard deviation (SD) from N=10 independent simulation runs.